Applied Physics Letters

Graphene fixed-end beam arrays based on mechanical exfoliation

Cite as: Appl. Phys. Lett. **98**, 253105 (2011); https://doi.org/10.1063/1.3594242
Submitted: 17 March 2011 . Accepted: 02 May 2011 . Published Online: 22 June 2011

Peng Li, Zheng You, Greg Haugstad, and Tianhong Cui

AIP Publishing

Graphene fixed-end beam arrays based on mechanical exfoliation

Peng Li,[1,3] Zheng You,[1,a)] Greg Haugstad,[2] and Tianhong Cui[1,3,b)]
[1]*Department of Precision Instruments and Mechanology, Tsinghua University, Beijing 100084, People's Republic of China*
[2]*Characterization Center, University of Minnesota, Minneapolis, Minnesota 55455, USA*
[3]*Department of Mechanical Engineering, University of Minnesota, Minneapolis, Minnesota 55455, USA*

(Received 17 March 2011; accepted 2 May 2011; published online 22 June 2011)

A low-cost mechanical exfoliation method is presented to transfer graphite to graphene for free-standing beam arrays. Nickel film or photoresist is used to peel off and transfer patterned single-layer or multilayer graphene onto substrates with macroscopic continuity. Free-standing graphene beam arrays are fabricated on both silicon and polymer substrates. Their mechanical properties are studied by atomic force microscopy. Finally, a graphene based radio frequency switch is demonstrated, with its pull-in voltage and graphene-silicon junction investigated. © *2011 American Institute of Physics*. [doi:10.1063/1.3594242]

Graphene is a two-dimensional honeycomb crystal of carbon atoms.[1] Its Young's modulus is about 1 TPa,[2] making it an excellent material for nanoelectromechanical systems.[3–6] The main approaches of graphene synthesis include mechanical exfoliation,[1] chemical vapor deposition,[7–11] graphene oxide reduction,[12–14] silicon carbide epitaxial growth,[15] etc. Mechanical exfoliation of highly oriented pyrolytic graphite (HOPG) provides the best quality graphene. Novoselov *et al.* used tape to peel graphite many times, and resulted in graphene. However, manipulation and transfer of graphene on a large scale is still a very challenging problem. Song *et al.*[16] used a sputter machine to deposit gold on prepatterned HOPG, and used the gold film to peel off graphene. Nevertheless, gold deposition by a sputter machine is not a low-cost method.

In this letter, a nickel film or a photoresist layer is used to exfoliate graphene patterns. First, patterns are formed on the surface of HOPG by photolithography followed by an oxygen plasma dry etching. Electroplating is used to grow a layer of nickel on HOPG surface. Before nickel electroplating, it is helpful to use a sputter for scanning electron microscope (SEM) to deposit a seed layer of gold on HOPG to increase the adhesion force. The electroplating solution, nickel sulfaminate, is heated to 58 °C with a dc of 20–30 mA. HOPG and stainless steel work as cathode and anode, respectively. A thermal releasing tape is pressed on HOPG, and peel off the nickel film together with graphene patterns. In order to remove thick graphene flakes, a new tape is used to peel the obtained film several times, before pressing the thermal releasing tape on substrate. The thermal releasing tape is removed through a heating process. The nickel layer is etched away, leaving graphene patterns on the substrate. Besides nickel, photoresist, is another good candidate. S1818 is spun on the prepatterned HOPG. When it is dry, a thermal releasing tape is used to peel graphene off, and transfer them onto a substrate. Photoresist is removed by acetone later. This method is inexpensive and easy to manipulate. In addition, the tape is not directly in contact with graphene or the substrate, therefore the graphene flakes have much less contaminants from the tape.

SEM image in Fig. 1(e) shows that the graphene patterns have a macroscopic continuity. More than 50 graphene stripes were investigated using atomic force microscopy (AFM): most patterns had thicknesses ranging from 1 nm to 5 nm. Out of 50 transfer printed graphene strips, More than 70% of patterns are almost complete. The depth of graphene patterns originally etched on HOPG is crucial to graphene thickness. Decreasing the depth can make graphene thinner.

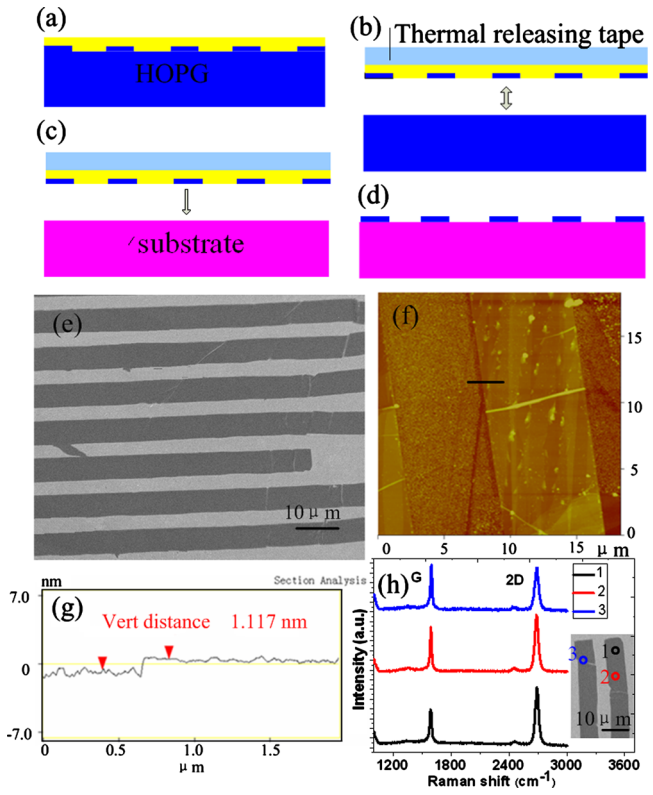

FIG. 1. (Color online) [(a)–(d)] Flow chart of graphene mechanical exfoliation. (a) Deposit nickel on patterned surface of HOPG. (b) Peel nickel layer with graphene flakes off from HOPG. (c) Press the tape on a heated substrate. (d) Remove tape and etch nickel. (e) SEM image of graphene strips. (f) AFM height image of a graphene stripe transferred onto S_iO_2. The black bar shows the scan distance. (g) The line scan using an AFM with graphene 1.2 nm thick. (h) Raman spectra of graphene from three different spots described in an SEM image.

a)Electronic mail: yz-dpi@mail.tsinghua.edu.cn.
b)Tel.: 1-612-626-1636. Electronic mail: tcui@me.umn.edu.

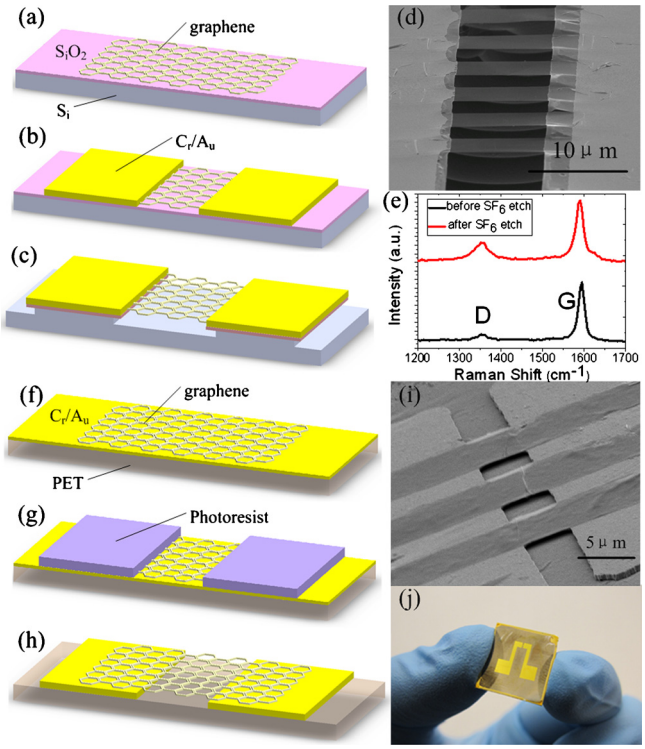

FIG. 2. (Color online) [(a)–(c)] Fabrication steps of a graphene beam array on silicon. (a) Transfer graphene on a S_iO_2/S_i substrate. (b) Fabricate gold pads using lift-off process. (c) HF vapor and SF_6 dry etching of S_iO_2 and S_i. (d) SEM image of a graphene beam array on silicon. (e) Raman spectra of the same graphene beam before and after dry etching. [(f)–(h)] Fabrication steps of a fixed-end graphene beam array on PET. (f) Transfer graphene on a PET substrate. (g) Use photoresist to define electrode pads. (h) Etch A_u and C_r by wet etching. Photoresist is moved by acetone, followed by a critical point drying. (i) SEM image of a graphene beam array on PET. (j) Photograph of a flexible suspended graphene device.

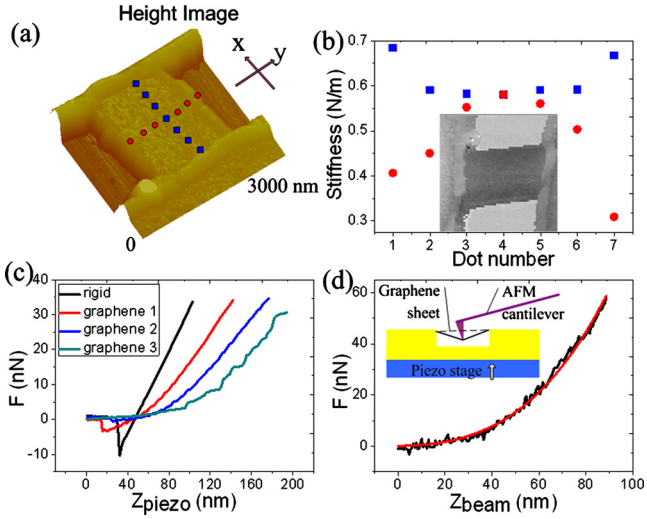

FIG. 3. (Color online) (a) AFM height image of a graphene beam. (b) Stiffness of 14 different spots described in an AFM height image. Inset shows force volume image (64 × 64 pixels). (c) Plot of cantilever force as a function of piezodisplacement for a hard substrate (black curve) and three different suspended beams. (d) Force verse deformation depth curve. The red line demonstrates that F is proportional to Z^3_{beam}. Inset shows a schematic of AFM cantilever indentation.

However, more cracks are observed. 15–20 nm is an optimum depth range. Figure 1(f) is AFM height image of one graphene stripe. Due to the exfoliation and transfer process, some ripples on graphene were observed. Curves in Fig. 1(h) are the Raman spectra of graphene from three different spots described in an SEM image. The 2D/G band ratio is much larger than that of bulk graphite. The Raman spectra further prove that our graphene patterns have only a few layers or even one layer. In addition, it shows no prominent D peaks, indicating far fewer defects in graphene derived by this approach.

After transferring graphene on S_iO_2/S_i, electrodes are fabricated by metal lift off process. Because the graphene patterns have a macroscopic continuity, an electron-beam photolithography can be replaced by a regular photolithography to largely decrease fabrication cost. After that, HF vapor is used to etch the S_iO_2, followed by an SF_6 plasma etching of S_i underneath. This dry etching method has a much higher yield compared with buffered oxide etchant wet etching. A prominent D peak appears in Raman spectra after the SF_6 plasma etching, implying the defects introduced by the this process.

A graphene beam array on a poly(ethylene terephthalate) (PET) was also fabricated. Before the graphene transfer, C_r and A_u are deposited on PET. Photoresist is spun on PET to define electrode pads. Sequentially, A_u and C_r are etched. During the wet etching process, photoresist is removed by acetone, followed by critical point drying. Figure 2(i) is SEM image of a graphene beam array on PET. We believe that this device may pave way for flexible graphene sensors, actuators, or even microsystems.

The mechanical properties of graphene beams were studied. AFM was used to acquire topographic images first, and then indent 64 × 64 grid of locations (force volume). The relationship between the graphene beam displacement, Z_{beam}, the piezostage movement, Z_{piezo}, and the cantilever deflection, Z_{tip}, is

$$Z_{beam} = Z_{piezo} - Z_{tip}. \tag{1}$$

The force, F, applied on the fixed-end beam is calculated as

$$F = K_{tip} Z_{tip}, \tag{2}$$

where K_{tip} is the spring constant of AFM cantilever. The force-Z data cube provided a 2D mapping of local stiffness. The stiffness reaches a minimum at the center with respect to the long beam axis but a maximum with respect to the short beam axis. This helps us to locate the center of the beam accurately. In Figure 3(c), the curve obtained on the rigid substrate was used as a reference. The other curves were obtained by pressing the same AFM tip to the center of three graphene beams having the same length but different thicknesses. Thinner graphene exhibits reduced stiffness, corresponding to lesser slope.

The relation between force and center displacement of a beam under a concentrated force is given by[17]

$$F = \frac{4wt}{l}\left(\frac{4Et^2}{l^2} + \frac{2EZ^2_{beam}}{3l^2} + \sigma\right) Z_{beam} \approx \frac{8wtE}{3l^3} Z^3_{beam} + \frac{4wt}{l}\sigma Z_{beam}, \tag{3}$$

where E is the graphene Young's modulus, σ is the initial stress, and l, w, and t are the length, width, and thickness of the beam, respectively. Because some ripples on graphene are observed with AFM, the graphene beam is not under large stress initially, therefore the Young's modulus is

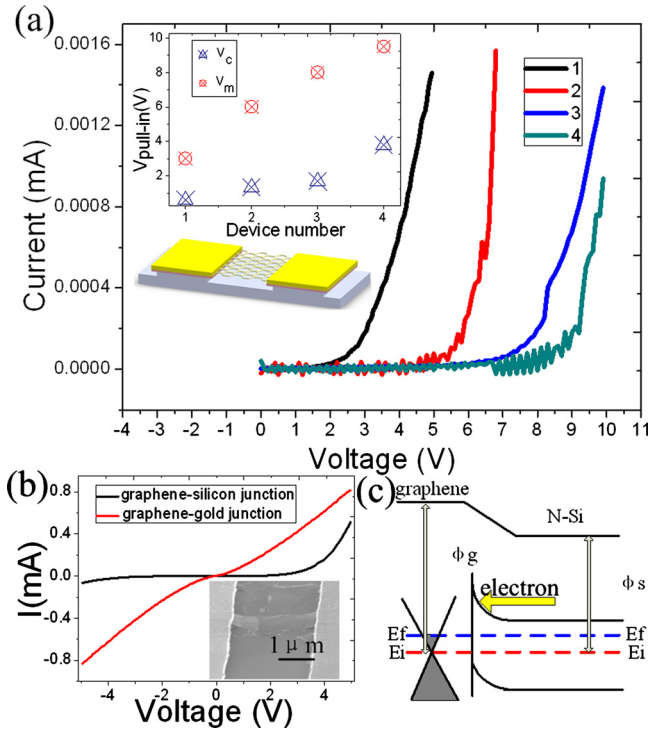

FIG. 4. (Color online) (a) I-V characteristics between the top and bottom contacts of four different graphene switches. Inset shows the measured pull-in voltages (V_m) and calculated pull-in voltages (V_c). (b) I-V characteristics of graphene-silicon junction and graphene-gold junction. Inset is an SEM image of a graphene beam collapsed onto an N-type silicon substrate. (c) Energy band diagram of a graphene-silicon junction.

$$E = \frac{3Fl^3}{8wtZ_{beam}^3}. \tag{4}$$

The red curve in Fig. 3(d) demonstrates that F is proportional to Z_{beam}^3. The Young's modulus of 0.8 TPa is derived on our graphene beam.

Graphene rf switches are demonstrated. Once the bias is larger than the pull-in voltage, graphene can be pulled to be in contact with the low resistivity silicon substrate, and a sharp increase in the current is observed. The spring constant of a fixed-end beam with a distributed load is

$$K = 32Ew\left(\frac{t}{l}\right)^3, \tag{5}$$

Therefore, pull-in voltage is

$$V_{pull\text{-}in} = \left(\frac{8Kg_0^3}{27\varepsilon lw}\right)^{1/2} = \left(\frac{256g_0^3Et^3}{27\varepsilon l^4}\right)^{1/2}, \tag{6}$$

where g_0 is the air gap between graphene and silicon, and ε is the vacuum permittivity.

Figure 4(a) shows the I-V curves of four graphene switches. The measured pull-in voltages are higher than those predicted by Eq. (6). That is because Eq. (5) is valid only for small deformations. When the deformation increases, the effective spring constant also increases, which contributes to a larger pull-in voltage.

The device switches several times before graphene is collapsed onto the substrate. The stiction occurs mainly from a short-range force between contact surfaces. The electrical property of stiction is examined by measuring the current through the graphene sheet and the silicon bottom. A prominent increase in current is observed when the potential on graphene is 3V higher than that on the n-type silicon substrate. A Schottky contact is formed between graphene and silicon. Electrons in silicon need an enough forward voltage to overcome the energy barrier to flow to the graphene side. Conversely, when graphene is collapsed onto gold substrate, the I-V curve is symmetric implying an Ohmic contact.

In summary, a low cost and simple method to produce graphene with a macroscopic continuity is reported. Graphene beam arrays both on silicon and PET substrates are fabricated. The mechanical properties of a graphene beam array are studied by AFM. Finally, graphene switches are demonstrated, with pull-in voltages and graphene-silicon junction investigated.

The authors acknowledge the assistance of fabrication and characterization from Nanofabrication Center and the Characterization Facility at the University of Minnesota.

[1]K. S. Novoselov, A. K. Geim, S. V. Morozov, D. Jiang, Y. Zhang, S. V. Dubonos, I. V. Grigorieva, and A. A. Firsov, Science **306**, 666 (2004).
[2]C. Lee, X. Wei, J. W. Kysar, and J. Hone, Science **321**, 385 (2008).
[3]J. S. Bunch, A. M. V. Zande, S. S. Verbridge, L. W. Frank, D. M. Tanenbaum, J. M. Parpia, H. G. Craighead, and P. L. McEuen, Science **315**, 490 (2007).
[4]C. Chen, S. Rosenblatt, K. I. Bolotin, W. Kalb, I. Kymissis, H. L. Stormer, T. F. Heinz, and J. Hone, Nat. Nanotechnol. **4**, 861 (2009).
[5]C. Gomez-Navarro, M. Burghard, and K. Kern, Nano Lett. **8**, 2045 (2008).
[6]S. Shivaraman, R. A. Barton, X. Yu, J. Alden, L. Herman, M. Chandrashekhar, J. Park, P. L. McEuem, J. M. Parpia, H. G. Craighead, and M. G. Spencer, Nano Lett. **9**, 3100 (2009).
[7]X. Li, W. Cai, J. An, S. Kim, J. Nah, D. Yang, R. Piner, A. Velamakanni, I. Jung, E. Tutuc, S. K. Banerjee, L. Colombo, and R. S. Ruoff, Science **324**, 1312 (2009).
[8]S. Bae, H. Kim, Y. Lee, X. Xu, J. S. Park, Y. Zheng, J. Balakrishnan, T. Lei, H. R. Kim, Y. Song, Y. J. Kim, K. S. Kim, B. H. Hong, and S. Lijima, Nat. Nanotechnol. **5**, 574 (2010).
[9]K. S. Kim, Y. Zhao, H. Jang, S. Y. Lee, J. M. Kim, K. S. Kim, J. H. Ahn, P. Kim, J. Y. Choi, and B. H. Hong, Nature (London) **457**, 706 (2009).
[10]P. W. Sutter, J. I. Flege, and E. A. Sutter, Nature Mater. **7**, 406 (2008).
[11]A. Reina, X. Jia, J. Ho, D. Nezich, H. Son, V. B. Bulovic, M. S. Dresselhaus, and J. Jing, Nano Lett. **9**, 30 (2009).
[12]Z. Wei, D. Wang, S. Kim, S. Y. Kim, Y. Hu, M. K. Yakes, A. R. Laracuente, Z. Dai, S. R. Marder, C. Berger, W. P. King, W. A. Heer, P. E. Sheehan, and E. Riedo, Science **328**, 1373 (2010).
[13]S. Park and R. S. Ruoff, Nat. Nanotechnol. **4**, 217 (2009).
[14]Y. Hernandez, V. Nicolosi, M. Lotya, F. M. Blighe, Z. Sun, I. Y. Mcgovern, B. Holland, M. B. Byren, Y. Gunko, J. J. Boland, P. Niraj, G. Duesberg, S. Krishnamurthy, R. Goodhue, J. Hitchison, V. Scardaci, A. C. F. Ferrari, and J. N. Coleman, Nat. Nanotechnol. **3**, 563 (2008).
[15]K. V. Emtsev, A. Bostwick, K. Horn, J. Jobst, G. L. Kellogg, L. Ley, J. L. McChesney, T. Ohta, S. A. Reshanov, J. Rohrl, E. Rotenberg, A. K. Schmid, D. Waldmann, H. B. Weber, and T. Seyller, Nature Mater. **8**, 203 (2009).
[16]L. Song, L. Ci, W. Gao, and P. M. Ajayan, ACS Nano **3**, 1353 (2009).
[17]W. Beitz and K. H. Grote, *Dubbel, Taschenbuch für den Maschinenbau* (Springer, Berlin, 2007).